

1 **Fracturing and crystal plastic behaviour of garnet under seismic stress in the**
2 **dry lower continental crust (Musgrave Ranges, Central Australia)**

3
4

5 Friedrich Hawemann^{1*}, Neil Mancktelow¹, Sebastian Wex¹, Giorgio Pennacchioni², Alfredo
6 Camacho³

7 1) Department of Earth Sciences, ETH Zurich, CH8092 Zurich, Switzerland
8 2) Department of Geosciences, University of Padova, Padova, Italy
9 3) Department of Geological Sciences, University of Manitoba, Winnipeg, Manitoba, R3T
10 2N2, Canada

11 * corresponding author friedrich.hawemann@erdw.ethz.ch

12

13 **Highlights**

- 14 • garnet deformed by fracturing and crystal-plasticity under dry lower crustal conditions
15 • Ca-diffusion profiles indicate multiple generations of fracturing
16 • diffusion is promoted along zones of higher dislocation density
17 • fracturing indicates transient high-stress (seismic) events in the lower continental
18 crust

19 **Abstract**

20 Garnet is a high strength mineral compared to other common minerals such as quartz and
21 feldspar in the felsic crust. In felsic mylonites, garnet typically occurs as porphyroclasts that

22 mostly evade crystal-plastic deformation, except under relatively high temperature
23 conditions. The microstructure of granulite facies garnet in felsic lower-crustal rocks of the
24 Musgrave Ranges (Central Australia) records both fracturing and crystal-plastic deformation.
25 Granulite facies metamorphism at ~ 1200 Ma generally dehydrated the rocks and produced
26 mm-sized garnets in peraluminous gneisses. A later ~ 550 Ma overprint under sub-eclogitic
27 conditions (600-700 °C, 1.1-1.3 GPa) developed mylonitic shear zones and abundant
28 pseudotachylite, coeval with the neocrystallization of fine-grained, high-calcium garnet. In
29 the mylonites, granulite-facies garnet porphyroclasts are enriched in calcium along rims and
30 fractures. However, these rims are locally narrower than otherwise comparable rims along
31 original grain boundaries, indicating contemporaneous diffusion and fracturing of garnet. The
32 fractured garnets exhibit internal crystal-plastic deformation, which coincides with areas of
33 enhanced diffusion, usually along zones of crystal lattice distortion and dislocation walls
34 associated with subgrain rotation recrystallization. Fracturing of garnet under dry lower
35 crustal conditions, in an otherwise viscously flowing matrix, requires transient high
36 differential stress, most likely related to seismic rupture, consistent with the coeval
37 development of abundant pseudotachylite.

38

39 **Keywords**

40 Garnet, Fracture, Crystal-Plasticity, Dry Lower Continental Crust, Pseudotachylite, Seismicity

41 **1 Introduction**

42 A fundamental problem in geology is the limited preservation of processes in the rock record.
43 This is especially the case for transient events, like earthquakes, traces of which are hardly

44 preserved due to later reworking. The best indicators for seismicity in the rock record are
45 pseudotachylytes (Sibson, 1975; Toy et al., 2011), although not every seismic event produces
46 frictional melts and, once formed, ductile creep or later brittle fracturing may erase most
47 traces (Sibson and Toy, 2006; Kirkpatrick and Rowe, 2013).

48 Garnet is stable in many metamorphic rocks over a large part of the pressure-temperature
49 space, is commonly preserved, and is suitable for a range of geothermobarometers and
50 geochronometers and their combination for geospeedometry (Lasaga, 1983; Caddick et al.,
51 2010; Baxter and Scherer, 2013). Being a high strength mineral (Karato et al., 1995; Wang and
52 Ji, 1999), both brittle and crystal plastic deformation are rarely observed in garnet when
53 compared to the common matrix minerals of the crust, such as quartz and feldspar. However,
54 Dalziel and Bailey (1968) already interpreted elongate garnets in high grade mylonites to be
55 the result of crystal plastic behaviour and advancements since then in electron microscopy,
56 and especially EBSD (electron backscatter diffraction), have allowed detailed investigation of
57 garnet textures (Kunze et al., 1993; Prior et al., 2000, 2002).

58 Experimental deformation of garnet indicates that differential stresses on the order of a few
59 GPa are required to produce shear fractures, and that the onset of crystal plastic behaviour
60 for strain rates typical of actively deforming regions ($10^{-12} - 10^{-15} \text{ s}^{-1}$; e.g. Behr and Platt, 2011)
61 should only occur at corresponding temperatures above ca. 750–640 °C (Karato et al., 1995;
62 Wang and Ji, 1999). The observation of fractured garnets in natural samples may therefore
63 be linked to seismic stresses, as suggested by Austrheim et al. (1996), who described
64 fracturing of garnets during pseudotachylyte formation and fluid-assisted eclogitization of
65 granulites. Trepmann and Stöckhert (2002) also interpreted the microstructure of fractured
66 and offset garnets as evidence for syn-seismic loading and post-seismic creep. More recently,

67 both brittle (Austrheim et al., 2017; Engi et al., 2017; Angiboust et al., 2017; Giuntoli et al.,
68 2018; Hawemann et al., 2018; Petley-Ragan et al., 2019) and associated crystal-plastic
69 behaviour (Austrheim et al., 2017; Petley-Ragan et al., 2019) of garnet has been related to
70 seismic events in lower continental crust or deeply subducted continental fragments. Papa et
71 al. (2018) interpreted similar deep-seated dilatant fracturing of garnet immediately adjacent
72 to pseudotachylite to be related to thermal shock due to frictional heating rather than to
73 damage associated with propagation of the seismic rupture. Konrad-Schmolke et al. (2007)
74 described enhanced diffusion of Mg along subgrain boundaries in garnet (but not of slow
75 diffusing elements, such as Ca, Ti and Y) from high pressure meta-granitoids of the deeply
76 subducted Sesia Zone (Western Alps). However, in contrast to more recent studies in the Sesia
77 Zone, which propose that precursor fracturing was crucial for dissolution–precipitation and
78 diffusion processes in garnet (Engi et al., 2018; Giuntoli et al., 2018), they considered that
79 there were no signs of crystal-plastic deformation in their garnet samples and concluded that
80 a diffusion-induced dislocation migration and/or diffusion-induced recrystallisation process
81 was responsible for development of the observed subgrain texture.

82 Here we present a study of garnet microstructures from lower crustal rocks of the Musgrave
83 Block in Australia, which:

- 84 (1) illustrates the close association between brittle and crystal-plastic deformation of
85 garnet under well-established pressure-temperature conditions;
- 86 (2) infers deformation mechanisms from the observed microstructure;
- 87 (3) explores the close link between deformation and diffusion in garnet;
- 88 (4) complements other independent observations indicating transient high stresses in the
89 lower crust.

91 **2 Geological setting**

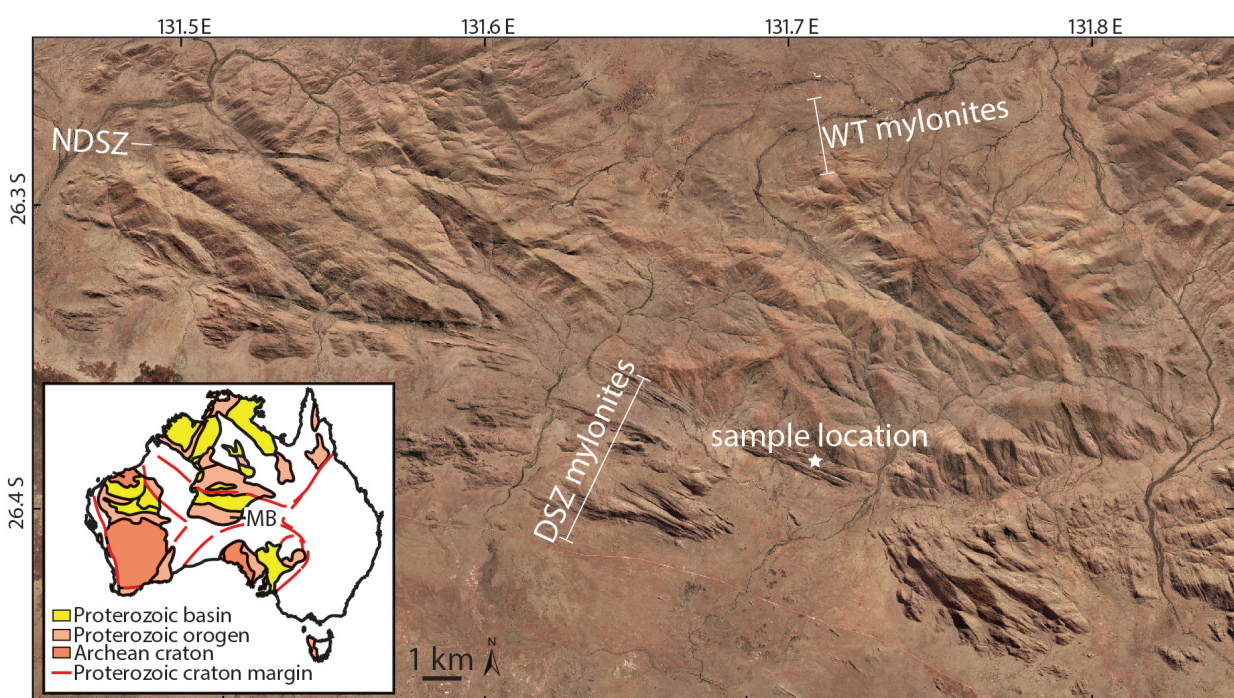
92 2.1 Regional geology

93 The Musgrave Block is located in an intraplate position close to the centre of the Australian
94 continent (inset Fig. 1). Amalgamation of the different cratonic blocks took place during the
95 Musgravian Orogeny (1120-1200 Ma), which pervasively overprinted ca. 1550 Ma gneisses
96 (Gray, 1978; Camacho and Fanning, 1995). The Petermann Orogeny (~550 Ma) produced a
97 series of crustal-scale fault zones, most prominently the Woodroffe Thrust and the Mann
98 Fault (Collerson et al., 1972; Major, 1973; Bell, 1978; Camacho and Fanning, 1995; Raimondo
99 et al., 2010; Hawemann et al., 2018, 2019; Wex et al., 2017, 2018, 2019). The south-dipping
100 Woodroffe Thrust has a top-to-the-north sense of shear, and juxtaposes the Fregon
101 Subdomain in the south (hanging wall) against the Mulga Park Subdomain in the north
102 (footwall). During the Musgravian Orogeny, the Mulga Park Subdomain attained amphibolite
103 facies conditions while the Fregon Subdomain reached granulite facies (Camacho and
104 Fanning, 1995; Scrimgeour et al., 1999; Scrimgeour and Close, 1999), and depleted the rocks
105 of OH-bearing minerals (Wex et al., 2018; Hawemann et al., 2018).

106 The Woodroffe Thrust hosts one of the largest occurrences of pseudotachylite worldwide
107 (Camacho et al., 1995), but all larger scale shear zones in the hanging wall also show abundant
108 pseudotachylite that developed under lower crustal conditions (Camacho, 1997; Hawemann
109 et al., 2018). Deformation in the Fregon Subdomain associated with the Petermann Orogeny
110 is concentrated along the sub-eclogitic (~650 °C, 1.2 GPa) Davenport Shear Zone and the
111 North Davenport Shear Zone (Fig. 1), with little discernible overprint of the earlier granulites
112 in between (Camacho et al., 1997). The Davenport Shear Zone is a WNW-ESE-striking, strike-

113 slip zone, with a near horizontal stretching lineation. Deformation inside the Davenport Shear
114 Zone itself is heterogeneous and strongly localized (Hawemann et al., 2019).

115



116

Figure 1: Airborne imagery of the study area with sample location (26.3849 S, 131.7067 E) in the Davenport Shear Zone (DSZ). NDSZ = North Davenport Shear Zone, WT = Woodroffe Thrust. Image from the Department of Primary Industries and Regions, South Australia (PIRSA), 2012. Inset: Location of the Musgrave Block (MB) in between the amalgamated Australian Cratons. Modified after Evans et al. (2010)

117

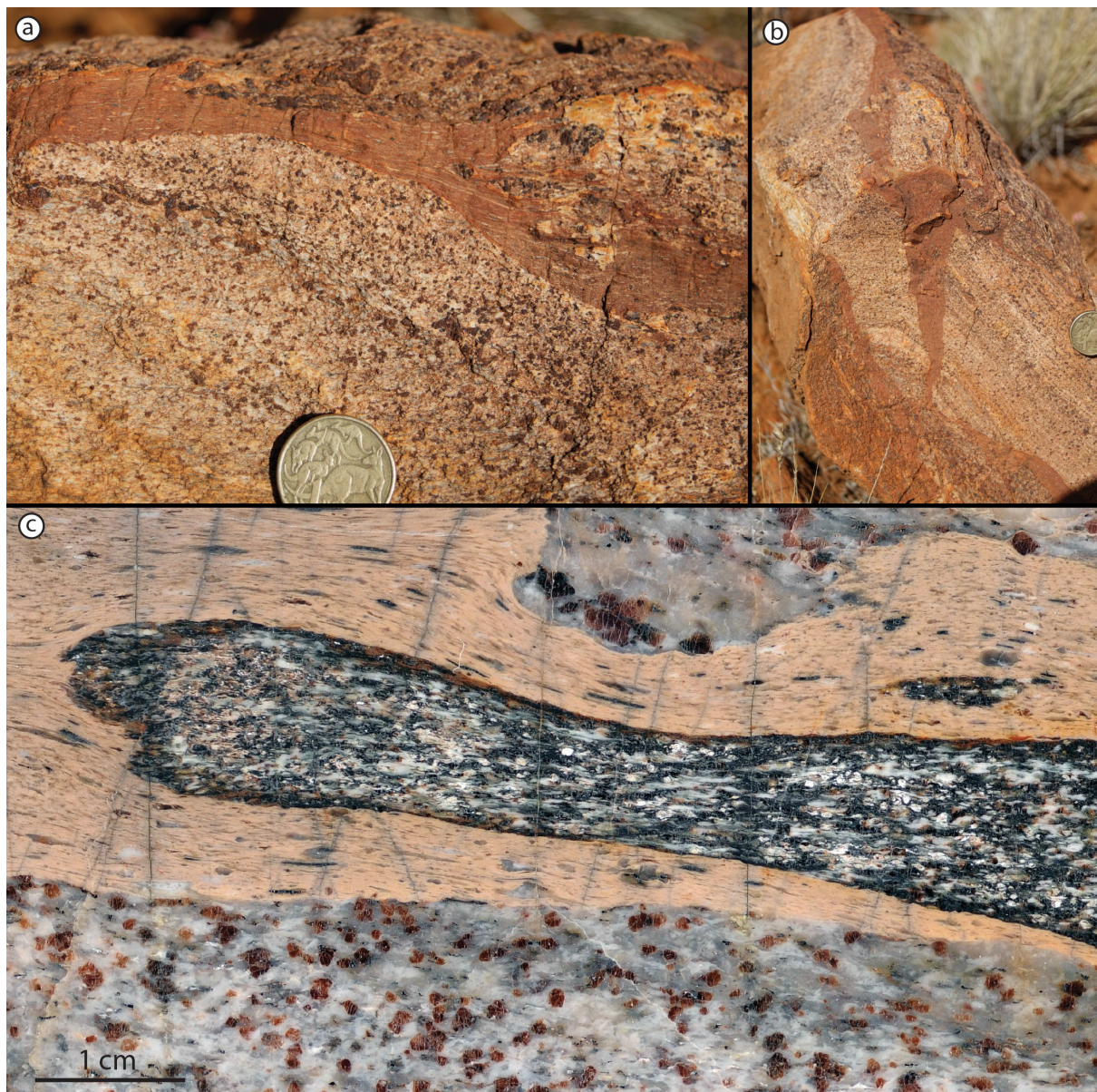
118 2.2 Sample description

119 Fractured garnet is ubiquitous in the Fregon Subdomain and is not exclusively found in
120 association with pseudotachylite veins. However, this study focuses on a representative
121 outcrop for which field relationships, metamorphic, and deformation conditions have been
122 well established (F68, Hawemann et al., 2018; 26.3849 S, 131.7067 E). This outcrop consists
123 of a quartzo-feldspathic mylonite with millimetre-sized, granulite facies garnets, and includes
124 multiple pseudotachylite veins and breccias. Pseudotachylites in the studied outcrop are

125 sheared, as indicated by elongated clasts (Fig. 2a, c), and show the same stretching lineation
126 as the host mylonite. The original discordant relationship to the host foliation is still
127 preserved, with the crosscutting relationship most obvious in sections perpendicular to the
128 stretching lineation (Fig. 2b).

129 The syn-mylonitic assemblage associated with the Petermann overprint of the felsic
130 granulites is Qz+Kfs+Pl+Gt+Bt+Ky+Ilm+Rt (mineral abbreviations following Whitney and
131 Evans, 2010), and is similar to that of the associated sheared pseudotachylite
132 (Qz+Kfs+Pl+Gt+Bt+Ky+Rt) (Hawemann et al., 2018). The fine-grained garnet growing within
133 the pseudotachylite gives the rock its macroscopic caramel-colour (Fig. 2). Larger fractured
134 garnets within the granulites are clearly recognizable in polished hand specimens (Fig. 2c) and
135 are very apparent in thin section (Fig. 3). The metamorphic conditions during shearing of this
136 pseudotachylite are estimated at ~600 °C and ~1.1 GPa (Fig. 7 of Hawemann et al., 2018).

137



138

Figure 2: Sheared pseudotachylyte in a view orthogonal to the foliation of host felsic mylonite, and looking perpendicular (a) and parallel (b) to the stretching lineation. c) Polished hand specimen of a sheared pseudotachylyte breccia with the caramel-coloured foliated pseudotachylyte matrix including elongated clasts and an elongate fragment of mafic granulite. The host rock shows millimetre-sized garnets with fractures. Plane of the polished surface is perpendicular to the foliation and parallel to the stretching lineation.

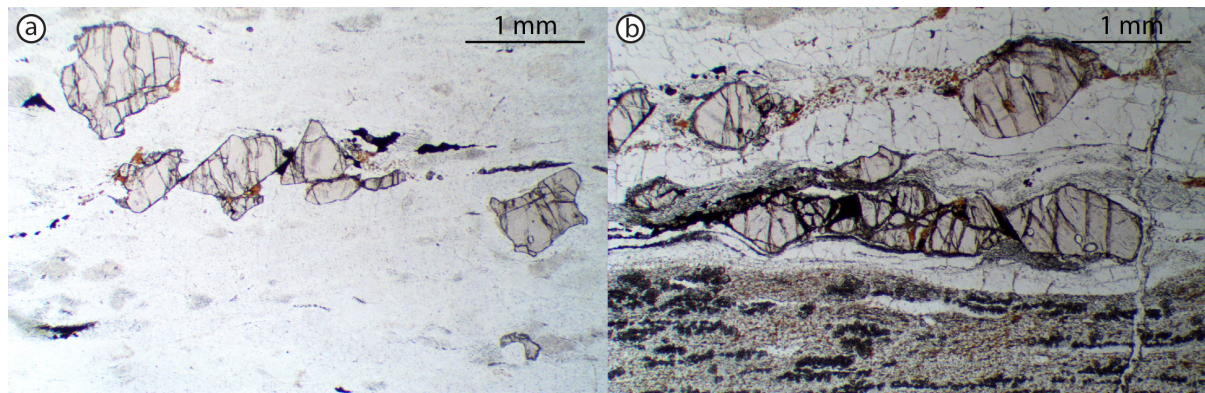
139

140 **3 Garnet microstructure and compositional variation**

141 **3.1 Optical microstructure**

142 Granulite facies garnet porphyroclasts in Musgravian peraluminous gneisses mylonitized
143 during the Petermann Orogeny are almost invariably fractured, irrespective of their proximity
144 to pseudotachylite (Fig. 3). Large garnet porphyroclasts (>1 mm) are typically slightly
145 elongated with their long axis parallel to the foliation, which is attributed at least partially to
146 resorption. Fractures in garnets often show offsets on the order of a few 100 µm. It is not
147 possible to determine whether these offsets are primarily due to the initial shear fracture or
148 result from subsequent sliding during ongoing ductile shear. Moreover, no consistent sense
149 of shear can be derived from the offsets (Fig. 3a, b). These discrete fractures are sub-planar,
150 commonly have a consistent orientation at a moderate angle to the foliation, and locally occur
151 in conjugate sets (Fig. 3b). Wide fractures are filled with biotite, kyanite and quartz (Fig. 4b).
152 A later generation of unfilled fractures, without any discernible offset, is oriented
153 perpendicular to both the foliation and stretching lineation (Fig. 3b). Garnet porphyroclasts
154 commonly contain rutile exsolution lamellae and inclusions of monazite and kyanite (Fig. A1).
155 The latter are present as aggregates with an overall prismatic shape, possibly representing
156 pseudomorphs after sillimanite (Camacho and Fitzgerald, 2010).

157



158

Figure 3: Thin section photomicrographs in plane polarized light of fractured garnets away from pseudotachylite (a), and close to sheared and recrystallized pseudotachylite in the lower part of the figure (b). The dark trails of grains elongated in the foliation of the sheared pseudotachylite are small new garnets. Section is perpendicular to the foliation and parallel to the stretching lineation.

159

160

161

162 3.2 Analytical techniques

163 Quantitative mineral compositions were measured with a JEOL JXA-8200 electron probe
164 micro-analyzer (EPMA), equipped with a tungsten filament, at the Institute of Geochemistry
165 and Petrology at ETH Zurich (Switzerland). Natural standards were used for quantification,
166 and, when available, natural garnet standards were preferred. To reach a spatial resolution
167 of about 1 µm, an acceleration voltage of 10 kV was set (Fig. 8 in Hofer and Brey, 2007).
168 Elemental maps were acquired using energy wavelength-dispersive spectrometers in parallel
169 for calcium, to increase the signal-to-noise ratio. Backscatter electron images (BSE), energy-
170 dispersive spectrometry (EDS) and electron backscatter diffraction (EBSD) mapping was
171 carried out on a Quanta 200F field emission gun (FEG) scanning electron microscope at the
172 ScopeM (Scientific Center for Optical and Electron Microscopy, ETH Zurich). EBSD maps were
173 collected with an acceleration voltage of 20 kV, a sample tilt of 70° and a working distance of
174 15 mm. Data were post-processed using chemical indexing with the software OIM 7 by EDAX.
175 When necessary, three different clean-up techniques were used: neighbour confidence index
176 correlation, neighbour orientation correlation and grain dilation. Point and map analyses, as
177 well as BSE images, were combined for correlation with optical microscope images in a QGIS-
178 project (Open Source Geospatial foundation). Two lamellae were cut with a focused ion beam
179 (FIB) for transmission electron microscopy (TEM). The microscope used for TEM is a Tecnai

180 F30 with a FEG source operated at 300 kV and equipped with a Gatan 794 MultiScan CCD
181 (ScopeM, ETH Zurich).

182 3.3 Compositional gradients

183 Granulite facies garnet has a homogeneous composition of X_{Alm} 0.54, X_{Pyp} 0.40, X_{Grs} 0.03, X_{Sps}
184 0.03, whereas garnet neocrystallized during the Petermann Orogeny is more Ca-rich (X_{Alm}
185 0.48, X_{Pyp} 0.28, X_{Grs} 0.22, X_{Sps} 0.02). Grain boundaries of granulite facies garnet and fractures
186 are decorated with a Ca-enriched rim, 20 to 40 μm wide (Fig. 4c). The length-scale for
187 variation in Fe (X_{Alm}) and Mg (X_{Pyp}) is identical to that for Ca (X_{Grs}), whereas the Mn content
188 (X_{Sps}) does not show any variation (Fig 4d). Neocrystallized garnet is present where the grain
189 boundary is in contact with, or close to, plagioclase. The outermost rim of remnant garnet has
190 the same composition as the neocrystallized garnet (Fig. 4d, profile 1). The granulite-facies
191 plagioclase is partially transformed to a more Na-rich plagioclase with needle shaped
192 inclusions of kyanite (bottom of Fig. 4e). This reaction provides Ca for the observed diffusion
193 into garnet (Camacho et al., 2009).

194 Along fractures across the porphyroclasts, the Ca enrichment is narrower than along the grain
195 boundaries and the grossular component only reaches up to about X_{Grs} 0.1 (Fig. 4d, profile 2).
196 Compositional gradients are also present around inclusions in garnet connected to the outer
197 garnet boundary, providing evidence of Ca diffusion along grain boundaries (right part of Fig.
198 4c, profile 3 in Fig 4d). Profile 4 (Fig. 4d) was measured next to a kyanite inclusion: the
199 diffusion length is still comparable to those of profiles 1-3, but Ca concentrations are much
200 lower. Ca probably diffused along fractures (invisible in the plane of the thin section) towards
201 the inclusion. In summary, the diffusion length at the original grain boundaries is maximized
202 where in contact with plagioclase, and otherwise constant at about 20 μm width. However,

203 variations in diffusion lengths do occur around garnet fragments, without any correlation with
204 the proximity to plagioclase, although the exact relationship in the third dimension is
205 unknown. Surfaces with limited diffusion can often be identified as fracture surfaces, which
206 were exposed to diffusion for a shorter time than original grain boundaries (Fig. 4e). Fractures
207 oriented perpendicular to the foliation and stretching lineation lack any signs of diffusion and
208 are therefore interpreted as later stage extensional fractures.

209 Some garnets display more complicated compositional patterns, with zones >100 µm of Ca
210 enrichment extending into the porphyroblast's interior, which are not associated with
211 fractures (e.g. the garnet fragment on the far right in Figure 4e). EBSD analysis highlights that
212 the three fragments in the right part of Figure 4e most likely originated from the same grain,
213 as they share a common rotation axis (Fig. 4f). The colours in the inverse pole figure map are
214 not solid, reflecting slight variations of orientation within the crystal. Furthermore, the image
215 quality map shows areas of suppressed Kikuchi patterns (grey value) suggestive of higher
216 dislocation density and therefore possible subgrain boundaries (Fig. 4f). The misorientation
217 angle map (Fig. 4g) reveals a complex pattern of varying crystal orientation (all within the
218 order of 5°) in the fragments, with very distributed zones connected to the edges of the
219 crystal, triangular-shaped zones of misorientation (upper left of Fig. 4g), and discrete zones
220 (lower right of Fig. 4g). The discrete zones of misorientation, about 5 µm wide, correlate well
221 with the Ca-enriched zones (compare Fig. 4e, f, garnet fragment on the right).

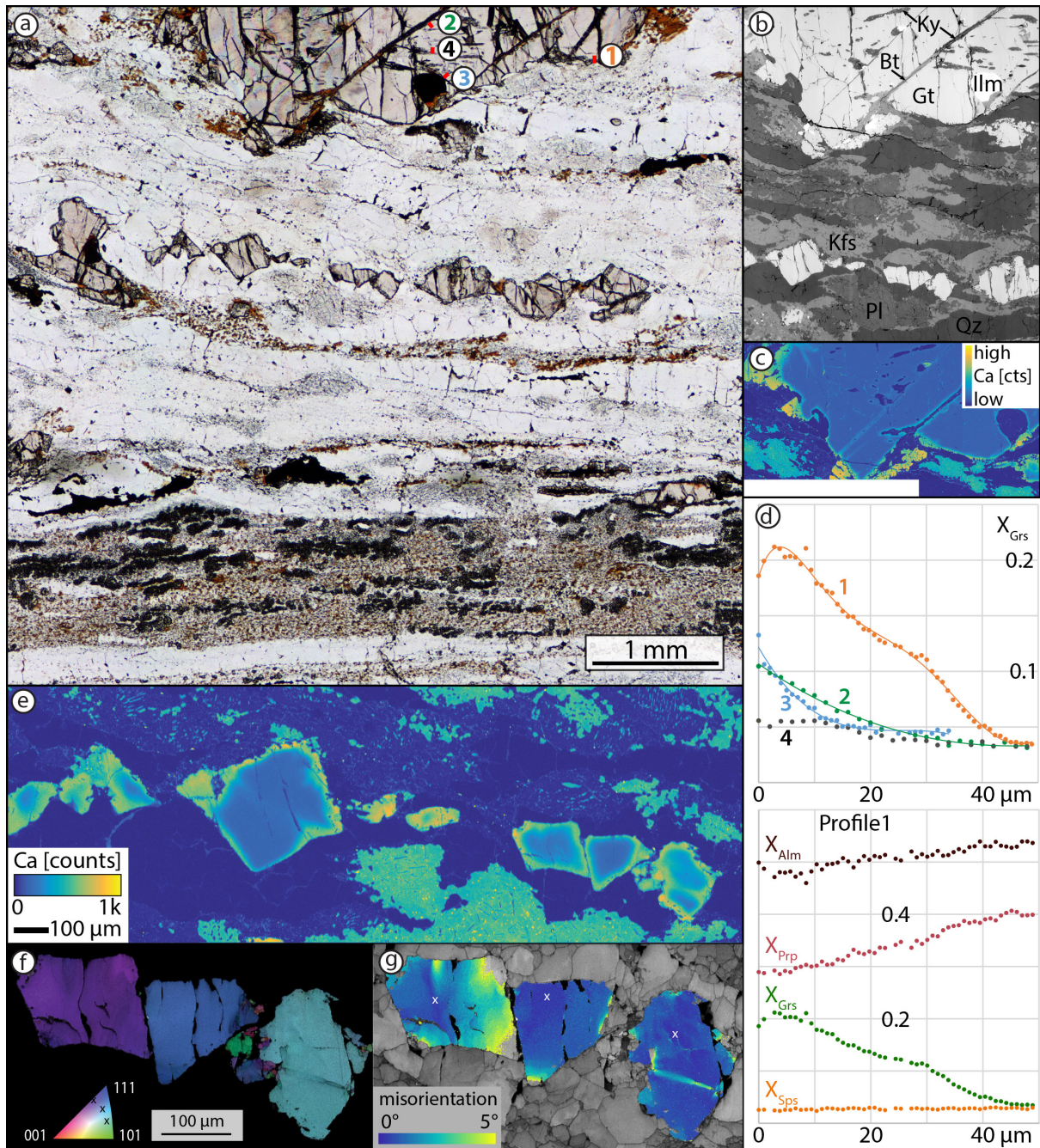
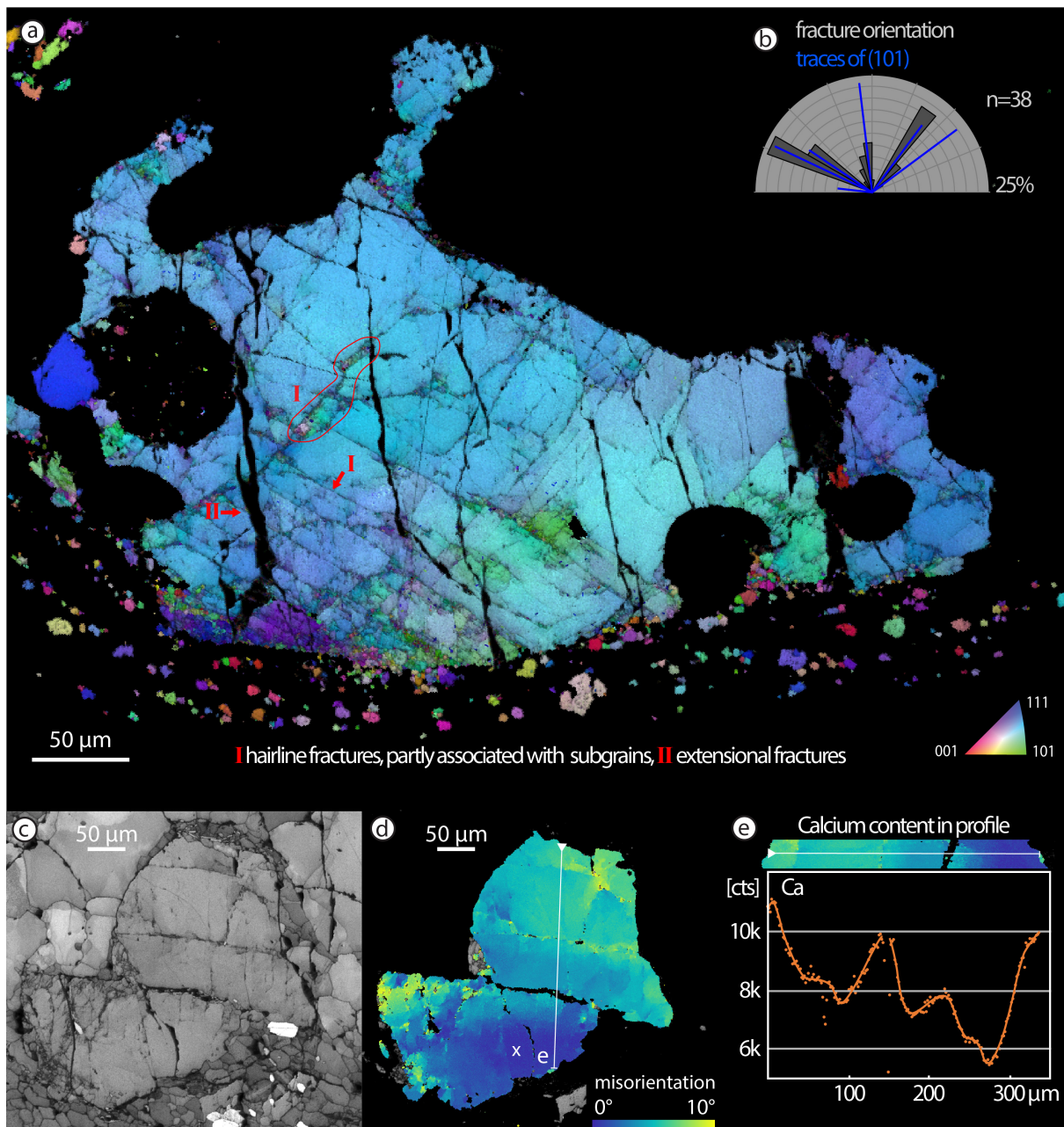


Figure 4: a) Plane polarized light image of thin section with fractured garnets and a pseudotachylite vein in the lower part of the image. b) BSE image of the upper area of (a), with same scale as (a). c) EPMA X-ray map for Ca reveals an enrichment in thin gradational rims along grain boundaries and fractures, and within neocrystallized garnet (euhedral, orange). d) Grossular component profiles indicated on (a) (profile lines are not to scale for the sake of visibility) and compositional profiles for four garnet end-members in profile 1. e) EPMA X-ray map for Ca for the garnet fragments in the center of (a). Note the uneven colours in the plagioclase and the blue kyanite needles. f) Inverse pole figure map with superimposed image quality map for garnet fragments shows a common rotation pole. g) Misorientation map relative to reference point for each fragment reveals internal lattice distortions.

224 3.4 Texture of deformed garnets

225 Two to three orientations of fractures are generally present in a single garnet crystal and
226 coincide with the trace of the (101)-plane derived from EBSD data (Fig. 5a, b). Fracture set (I)
227 in the example of Figure 5a is often associated with a relative rotation of both sides, as visible
228 from the difference in colour. In the lower part of the grain, where the fracture density is very
229 high, more subgrains are present. The subgrain spatial density increases towards the original
230 grain boundary and some subgrains are “eroded” by ductile shearing and strung out along the
231 foliation. This demonstrates that ductile shearing outlasted subgrain formation and
232 fracturing. The fractures described above are all crosscut by extensional fractures (set III in
233 Fig. 5a), oriented perpendicular to the stretching lineation and foliation, which do not show
234 any associated distortion of the crystal lattice.

235 The garnet porphyroblast of Figure 5c shows a central fracture as well as a set of two other
236 parallel fractures. The central fracture is the only one with significant offset and is filled with
237 kyanite and quartz. This fracture displays misorientations of more than 5° towards the right-
238 hand side of the scan, but none towards the left-hand side. In the lower left corner of the
239 fragment, subgrains are observed with misorientations, relative to the average orientation,
240 typically in the range of 10°. Misorientation axes are often parallel to (111) and (101). The
241 lowermost fragment shows a wide zone of progressive rotation. The chemical profile in Figure
242 5e shows the highest Ca counts towards the boundaries of the porphyroclasts and, internally,
243 towards two fractures. The larger fracture with apparent offset of the two garnet fragments
244 exhibits a less well-developed zone of Ca enrichment when compared to the tight fracture
245 with introduced lattice distortion.



246

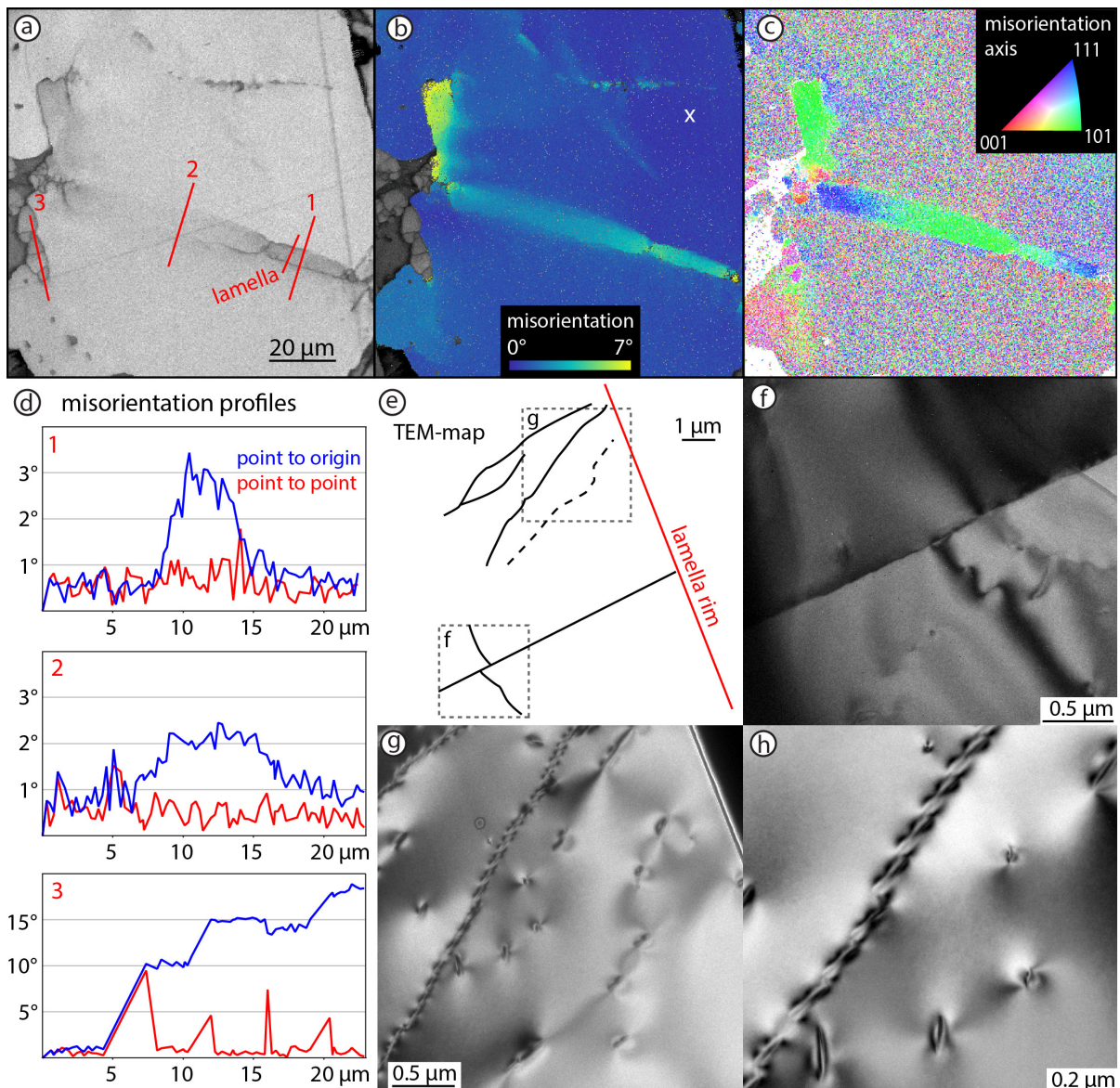
Figure 5: a) Inverse pole figure map of fractured garnet with three dominant orientations of fractures. b) Rose diagram correlating traced fracture orientations and (101)-planes for garnet in (a). c) Image quality map of a fragmented garnet with subgrains. d) Misorientation plot (with respect to the point marked with the white x) shows long wavelength bending in the lower fragment and distortion in the crystal lattice induced by a fracture in the upper fragment. e) EDS-calcium counts for the profile marked as a thin white line in (d).

247

248

249 3.5 TEM investigations

250 The garnet fragment of Figure 4g was further investigated using TEM, as it includes a narrow
251 zone of misorientation without fractures and is therefore suitable for preparation of FIB-
252 lamellae. As visible in Figure 6a (around profile 1), the image quality map shows a well-defined
253 narrow, darker grey band, possibly indicating high dislocation density. The zone is even more
254 evident in the misorientation plot (Fig. 6b) and changes from about 5 µm wide, with discrete
255 boundaries to the right, to a wider (> 10 µm) band towards the left of the image. In the upper
256 left part of the image, a subgrain boundary with > 5° misorientation transitions into a zone of
257 gradual misorientation. The misorientation axis is consistently parallel to (101) with minor
258 rotation around (111) (Fig. 6c, Fig. A2). Misorientation profiles reveal a slight asymmetry
259 within the narrow band, where the lower boundary appears to be sharper. Misorientation
260 changes more gradually within the wider portion of the misorientation band. Locally,
261 subgrains developed with discrete boundaries, documenting a misorientation of usually
262 around 5-10° (profile 3 in Fig. 6d). The FIB-lamella was cut across the narrow band of
263 misorientations (Fig. 6e). The lower boundary corresponds to a narrow discrete zone, without
264 visible dislocations (Fig. 6f). The upper boundary is marked by a series of dislocation walls and
265 only a few free dislocations are visible, which are often organized in arrays (Fig. 6g, h). The
266 existence of dislocation walls and subgrain boundaries indicates recovery by dislocation climb
267 (e.g., Hobbs, 1968; Passchier and Trouw, 2005).



268

Figure 6: a) Image quality map of the garnet fragment (compare Fig. 4f) with darker zones that can be interpreted as areas of high dislocation density and location of the FIB-lamella. *b)* Misorientation plot with respect to the reference point (marked with the white x) shows a discrete zone of misorientation, which has discrete boundaries in the right part of the image, but is more distributed towards the left. *c)* Misorientation axis plot with respect to the average orientation of the grain shows a consistent rotation around the (101) and (111) axes. For pole figure plots, see Fig. A2. *d)* Misorientation profiles indicated in *a*), for (1) the narrow zone, (2) the more distributed zone and (3) for subgrains. *e)* Overview sketch of the FIB-lamella used for TEM-analysis for correlation with the EBSD data. *f)* Sharp contrast boundary in the lower part of the lamella. *g)* Two dislocation walls with a few free dislocations, which are partly linking up parallel to the dislocation walls. *h)* Detail of the centre of (*g*)

269

270

271 **4 Discussion**

272 Garnets in this study show evidence for both brittle and ductile deformation under relatively
273 low temperatures of about 600 °C, as inferred from synchronous diffusion and ductile
274 shearing of pseudotachylite (Hawemann et al., 2018). This is below the experimentally
275 determined values for the onset of crystal-plastic deformation of garnet (Wang and Ji, 1999)
276 at the higher strain rates considered typical of mylonitic shear zones ($> 10^{-14} \text{ s}^{-1}$). In contrast
277 to experiments, many natural examples (Vollbrecht et al., 2006; Bestmann et al., 2008;
278 Austrheim et al., 2017) indicate crystal plasticity of garnet at lower temperatures between
279 650 °C and 700 °C.

280 The presence of microstructures and textures consistent with dislocation climb and recovery,
281 as well as subgrain rotation, in garnet at around 600 °C is in agreement with previous studies
282 (Bestmann et al., 2008; Massey et al., 2011). No evidence for grain boundary sliding is
283 observed, since subgrains show rotation around a specific crystallographic axis. Rotation
284 around (111) and (101) is in accordance with the slip systems described by Voegelé et al.
285 (1998).

286 Multiple generations of overprinting fractures with different orientation demonstrate
287 repeated fracturing events. Extensional fractures do not show any induced lattice distortion
288 or diffusion and therefore occurred after the temperature had decreased to values too low
289 for diffusion (Camacho et al., 2009), possibly during exhumation (compare Prior, 1993 and Ji
290 et al., 1997).

291 In contrast to the observations of Austrheim et al. (2017), Papa et al. (2018) and Petley-Ragan
292 et al. (2019) from other examples in the deep continental crust, no “explosive fracturing”,
293 “shattering” or “fragmentation” of garnet is observed in relict porphyroclasts immediately

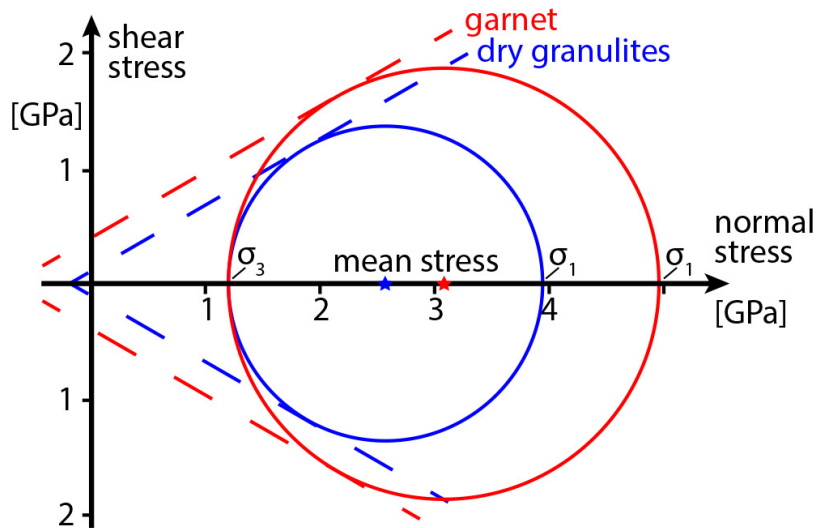
adjacent to pseudotachylite. The fractures described here are generally planar and often consistently oriented, in some cases showing single and conjugate shear offsets. Fractured garnet is not restricted to the boundary with pseudotachylite and is still present even in samples without pseudotachylite, where the nearest pseudotachylite is possibly many metres or more away. Fracturing in this case cannot be related to thermal shock (Papa et al., 2018) or localized high stress due to (seismic) fracture propagation (Austrheim et al., 2017; Petley-Ragan et al., 2019), but must reflect a larger scale distribution of differential stresses in the lower crust that were, at least transiently, high enough to cause brittle garnet failure (Hawemann et al., 2019). This could be due to stress pulses from earthquakes in the shallower brittle regime (Trepmann and Stöckhert, 2002; Ellis and Stöckhert, 2004; Jamtveit et al., 2018a, b; Jamtveit et al., in press) or a more local, lower crustal source due to jostling of less-deformed strong blocks within an irregular shear zone network (Hawemann et al., 2019).

The narrower Ca diffusion profiles on some fractures relative to garnet rims and crosscutting relationships suggest that fracturing was recurrent under sub-eclogite facies metamorphic conditions, as also indicated by the occasional presence of kyanite in some fractures. The presence of kyanite needles and the absence of zoisite/clinozoisite or epidote, as a breakdown product of plagioclase during sub-eclogitic metamorphism (Fig. 3b), indicate relatively dry lower crustal conditions (Hawemann et al., 2018). According to Wayte et al. (1989), this indicates a water activity of < 0.004, calculated for rocks of comparable composition and P-T conditions. However, new biotite did form in fractures across relict garnet, so conditions were probably not strictly anhydrous. The sheared and recrystallized pseudotachylite developed a similar synkinematic assemblage as the host mylonite, demonstrating that there is also no marked partitioning of water into the frictional melt, which implies little free or bound water available in the original source rock (e.g. Wex et al.,

318 2018). The effect of pore-fluid pressure on the effective confining pressure must therefore
319 have been negligible.

320 As reported in Hawemann et al. (2019), the dynamically recrystallized quartz grain size and
321 microstructure in the host rock mylonites indicates that long-term flow stresses were not
322 particularly high, on the order of less than 10 MPa. The ambient pressure of ca. 1.1-1.2 GPa
323 determined for the host rocks should therefore be close to the lithostatic value (Mancktelow,
324 2008). Figure 7 shows a simple linear plot of the Mohr-Coulomb failure criterion for an angle
325 of internal friction of 30° (coefficient $\mu = 0.6$), a lithostatic load of 1.2 GPa, and no pore fluid
326 pressure. This plot is only qualitative, since the angle of internal friction could decrease
327 towards higher pressure (Shimada et al., 1983). However, the summary of experimental
328 results in Byerlee (1978) indicates that there may be little change at least up to pressures
329 similar to those considered here. It follows that the differential stress for fracture initiation
330 must have been of the same order as the confining pressure (Fig. 7). As discussed in detail in
331 Hawemann et al. (2019), such high differential stresses, leading to garnet fracture and the
332 development of abundant pseudotachylite, can only have been transient and presumably
333 related to repeated short-term seismic events in the lower continental crust (Hawemann et
334 al., 2018; Jamtveit et al, 2018a, b; Menegon et al., 2017). The lack of shattered garnet adjacent
335 to pseudotachylite in these samples may reflect drier conditions relative to those in the
336 Bergen Arc (Austrheim et al., 2017) and Mont Mary (Papa et al., 2018). The samples studied
337 could therefore represent one end-member of the lower continental crust, where
338 deformation occurs without the initial presence or influx of free water during fracturing and
339 subsequent crystal-plastic deformation.

340



341

Figure 7: Mohr circles for fracturing of dry granulites and garnet at 1.2 GPa lithostatic load

342

343 5 Conclusions

344 In dry lower continental crust deformed under conditions of ca. 600 °C and 1.1 GPa, garnet
 345 shows both single and conjugate sets of shear fractures, fractures with associated subgrains
 346 and induced lattice damage around fractures, subgrain formation without fracturing, and
 347 late-stage extensional fractures. Most of these fractures show a strong crystallographic
 348 control, with fracturing preferentially occurring along the (101) planes of garnet. Dynamic
 349 recrystallization is evident from inferred subgrain rotation recrystallization and recovery is
 350 manifested by the presence of dislocation walls. The observed microstructures of garnets are
 351 interpreted to record transient high stresses during deep seismic events in the lower crustal
 352 Fregon Subdomain. This is also indicated by the abundant occurrence of pseudotachylite
 353 developed under similar lower crustal conditions and, possibly, by the variability of
 354 recrystallized quartz grain sizes including values down to a few micrometres (Hawemann et
 355 al. 2009b). The studied example represents one end-member of lower continental crustal
 356 behaviour where, because of earlier metamorphic dehydration and the intracratonic position

357 well removed from the plate margin, rocks were initially dry and water was not introduced
358 during fracturing and crystal-plastic deformation.

359 **Author contributions**

360 All authors listed took part in at least two of the three field seasons. NM assisted FH in the data
361 collection and interpretation. AC's and GP's knowledge in the field of garnet deformation and diffusion
362 processes were crucial in preparing the manuscript. SW contributed to the microprobe and SEM work.
363 FH prepared the manuscript with contributions from all co-authors.

364 **Competing interests**

365 The authors declare that they have no conflict of interest.

366

367 **Acknowledgements**

368 We want to thank Matthias Konrad-Schmolke and an anonymous reviewer for their critical
369 comments which improved the manuscript. We gratefully acknowledge permission granted to
370 work on the Anangu Pitjantjatjara Yankunytjatjara Lands (APY) to carry out our field work in
371 the area. The Northern Territory Geological Survey (NTGS) and Basil Tikoff (Department of
372 Geoscience, University of Wisconsin) are thanked for their logistical support and the Nicolle
373 family of Mulga Park station for their hospitality. The Scientific Center for Optical and Electron
374 Microscopy (ScopeM) provided the facilities for the scanning electron microscopy work, and
375 help by Karsten Kunze, Luiz Morales and Fabian Gramm is especially acknowledged. Luca
376 Menegon is thanked for his review of the first author's doctoral thesis. This project was
377 financed by the Swiss National Science Foundation (SNF) grant 200021_146745 and by the
378 University of Padova (BIRD175145/17: The geological record of deep earthquakes: the
379 association pseudotachylite-mylonite).

380

381 **Data Availability**

382 All data used in this paper can be accessed through the depository of the Open Science

383 Framework here: <https://osf.io/yrzgh/>

384

385 **References**

386 Austrheim, H., Erambert, M. and Boundy, T. M.: Garnets recording deep crustal earthquakes, Earth
387 and Planetary Science Letters, 139(1–2), 223–238, doi:10.1016/0012-821X(95)00232-2, 1996.

388 Austrheim, H., Dunkel, K. G., Plümper, O., Ildefonse, B., Liu, Y. and Jamtveit, B.: Fragmentation of
389 wall rock garnets during deep crustal earthquakes, *Science Advances*, 3(2), e1602067,
390 doi:10.1126/sciadv.1602067, 2017.

391 Angiboust, S., Yamato, P., Hertgen, S., Hyppolito, T., Bebout, G.E., Morales, L.: Fluid pathways and
392 high-P metasomatism in a subducted continental slice (Mt. Emilius klippe, W. Alps), *Journal of*
393 *Metamorphic Geology*, 35, 471–492, 2017.

394 Baxter, E. F. and Scherer, E. E.: *Garnet Geochronology: Timekeeper of Tectonometamorphic*
395 *Processes*, *Elements*, 9(6), 433–438, doi:10.2113/gselements.9.6.433, 2013.

396 Behr, W.M., Platt, J.P.: A naturally constrained stress profile through the middle crust in an
397 extensional terrane. *Earth and Planetary Science Letters* 303, 181–192, 2011.

398 Bell, T. H.: Progressive deformation and reorientation of fold axes in a ductile mylonite zone: the
399 Woodroffe thrust, *Tectonophysics*, 44(1), 285–320, 1978.

400 Bestmann, M., Habler, G., Heidelbach, F. and Thöni, M.: Dynamic recrystallization of garnet and
401 related diffusion processes, *Journal of Structural Geology*, 30(6), 777–790,
402 doi:10.1016/j.jsg.2008.02.007, 2008.

403 Caddick, M. J., Konopasek, J. and Thompson, A. B.: Preservation of Garnet Growth Zoning and the
404 Duration of Prograde Metamorphism, *Journal of Petrology*, 51(11), 2327–2347,
405 doi:10.1093/petrology/egq059, 2010.

406 Camacho, A. and Fanning, C. M.: Some isotopic constraints on the evolution of the granulite and
407 upper amphibolite facies terranes in the eastern Musgrave Block, central Australia, *Precambrian*
408 *Research*, 71(1), 155–181, 1995.

409 Camacho, A. and Fitz Gerald, J. D.: Misidentification of oxide phases and of twinned kyanite:
410 implications for inferred P-T histories of the Musgrave Block, central Australia, *Journal of the Virtual*
411 *Explorer*, 35, doi:10.3809/jvirtex.2011.00275, 2010.

- 412 Camacho, A., Vernon, R. H. and Fitz Gerald, J. D.: Large volumes of anhydrous pseudotachylite in the
413 Woodroffe Thrust, eastern Musgrave Ranges, Australia, *Journal of Structural Geology*, 17(3), 371–
414 383, 1995.
- 415 Camacho, A., Compston, W., McCulloch, M. and McDougall, I.: Timing and exhumation of eclogite
416 facies shear zones, Musgrave Block, central Australia, *J. metamorphic Geol.*, 15, 735–751, 1997.
- 417 Camacho, A., Yang, P. and Frederiksen, A.: Constraints from diffusion profiles on the duration of
418 high-strain deformation in thickened crust, *Geology*, 37(8), 755–758, 2009.
- 419 Collerson, K. D., Oliver, R. L. and Rutland, R. W. R.: An example of structural and metamorphic
420 relationships in the Musgrave orogenic belt, central Australia, *Journal of the Geological Society of*
421 *Australia*, 18(4), 379–393, doi:10.1080/00167617208728776, 1972.
- 422 Dalziel, I. W. D. and Bailey, S. W.: Deformed garnets in a mylonitic rock from the Grenville Front and
423 their tectonic significance, *American Journal of Science*, 266(7), 542–562, doi:10.2475/ajs.266.7.542,
424 1968.
- 425 Ellis, S., Stöckhert, B.: Elevated stresses and creep rates beneath the brittle-ductile transition caused
426 by seismic faulting in the upper crust. *Journal of Geophysical Research*, 109, B05407, 2017.
- 427 Engi, M., Giuntoli, F., Lanari, P., Burn, M., Kunz, B. E., and Bouvier, A.-S.: Pervasive eclogitization due
428 to brittle deformation and rehydration of subducted basement: Effects on continental recycling?,
429 *Geochemistry Geophysics Geosystems*, 19, <https://doi.org/10.1002/2017GC007215>, 2018.
- 430 Evins, P. M., Smithies, R. H., Howard, H. M., Kirkland, C. L., Wingate, M. T. D. and Bodorkos, S.:
431 Redefining the Giles Event within the setting of the 1120-1020 Ma Ngaanyatjarra Rift, West
432 Musgrave Province, Central Australia, *Geological Society of Western Australia*, East Perth, W.A.,
433 2010.
- 434 Gray, C. M.: Geochronology of granulite - facies gneisses in the western Musgrave Block, Central
435 Australia, *Journal of the Geological Society of Australia*, 25(7–8), 403–414,
436 doi:10.1080/00167617808729050, 1978.
- 437 Giuntoli, F., Lanari, P., and Engi, M.: Deeply subducted continental fragments – Part 1: Fracturing,
438 dissolution–precipitation, and diffusion processes recorded by garnet textures of the central Sesia
439 Zone (western Italian Alps), *Solid Earth*, 9, 167–189, <https://doi.org/10.5194/se-9-167-2018>, 2018.
- 440 Hawemann, F., Mancktelow, N. S., Wex, S., Camacho, A. and Pennacchioni, G.: Pseudotachylite as
441 field evidence for lower-crustal earthquakes during the intracontinental Petermann Orogeny
442 (Musgrave Block, Central Australia), *Solid Earth*, 9(3), 629–648, doi:10.5194/se-9-629-2018, 2018.
- 443 Hawemann, F., Mancktelow, N. S., Pennacchioni, G., Wex, S. and Camacho, A.: Weak and slow,
444 strong and fast: How shear zones evolve in a dry continental crust (Musgrave Ranges, Central
445 Australia), *Journal of Geophysical Research: Solid Earth*, doi:10.1029/2018JB016559, 2019.
- 446 Hobbs, B.E.: Recrystallisation of single crystals of quartz. *Tectonophysics*, 6, 353-401, 1968.
- 447 Hofer, H. E. and Brey, G. P.: The iron oxidation state of garnet by electron microprobe: Its
448 determination with the flank method combined with major-element analysis, *American*
449 *Mineralogist*, 92(5–6), 873–885, doi:10.2138/am.2007.2390, 2007.
- 450 Jamtveit, B., Ben-Zion, Y., Renard, F., Austrheim, H.: Earthquake-induced transformation of the lower
451 crust. *Nature* 556, 487-491, 2018a.

- 452 Jamtveit, B., Moulas, E., Andersen, T.B., Austrheim, H., Corfu, F., Petley-Ragan, A., Schmalholz, S.M.:
453 High pressure metamorphism caused by fluid induced weakening of deep continental crust.
454 Scientific Reports, 8, 17011, 2018b.
- 455 Jamtveit, B., Petley-Ragan,A., Incel, S., Dunkel, K.G., Aupart,C., Austrheim, H., Corfu, F., Menegon, L.,
456 Renard, F: The effects of earthquakes and fluids on the metamorphism of the lower continental
457 crust, Journal of Geophysical Research: Solid Earth, doi:10.1029/2018jb016461, in press.
- 458 Ji, S., Zhao, P. and Saruwatari, K.: Fracturing of garnet crystals in anisotropic metamorphic rocks
459 during uplift, Journal of Structural Geology, 19(5), 603–620, 1997.
- 460 Karato, S., Wang, Z., Liu, B. and Fujino, K.: Plastic deformation of garnets: systematics and
461 implications for the rheology of the mantle transition zone, Earth and Planetary Science Letters,
462 130(1–4), 13–30, 1995.
- 463 Kirkpatrick, J. D. and Rowe, C. D.: Disappearing ink: How pseudotachylites are lost from the rock
464 record, Journal of Structural Geology, 52, 183–198, doi:10.1016/j.jsg.2013.03.003, 2013.
- 465 Konrad-Schmolke, M., O'Brien, P. J., Heidelbach, F.: Compositional reequilibration of garnet: the
466 importance of sub-grain boundaries. European Journal of Mineralogy 19, 431–438, 2007.
- 467 Kunze, K., Wright, S. I., Adams, B. L. and Dingley, D. J.: Advances in automatic EBSP single orientation
468 measurements, Texture, Stress, and Microstructure, 20(1–4), 41–54, 1993.
- 469 Lasaga, A. C.: Geospeedometry: an extension of geothermometry, in Kinetics and equilibrium in
470 mineral reactions, pp. 81–114, Springer. [online] Available from:
471 http://link.springer.com/chapter/10.1007/978-1-4612-5587-1_3 (Accessed 28 May 2017), 1983.
- 472 Major, R. B.: Explanatory Notes for the Woodroffe 1: 250 000 Geological Map SG/52-12 (1st
473 ed.). Adelaide, Australia: Geological Survey of South Australia, 1973.
- 474 Massey, M. A., Prior, D. J. and Moecher, D. P.: Microstructure and crystallographic preferred
475 orientation of polycrystalline microgarnet aggregates developed during progressive creep, recovery,
476 and grain boundary sliding, Journal of Structural Geology, 33(4), 713–730,
477 doi:10.1016/j.jsg.2010.12.009, 2011.
- 478 Menegon, L., Pennacchioni, G., Malaspina, N., Harris, K., Wood, E.: Earthquakes as precursors of
479 ductile shear zones in the dry and strong lower crust. Geochemistry, Geophysics, Geosystems, 18.
480 <https://doi.org/10.1002/2017GC007189>, 2017.
- 481 Papa, S., Pennacchioni, G., Angel, R. J. and Faccenda, M.: The fate of garnet during (deep-seated)
482 coseismic frictional heating: The role of thermal shock, Geology, 46(5), 471–474,
483 doi:10.1130/G40077.1, 2018.
- 484 Passchier, C.W., Trouw, R.A.J.: Microtectonics (2nd Edition), Springer, Heidelberg, 366 pp., 2005.
- 485 Petley-Ragan, A., Dunkel, K. G., Austrheim, H., Ildefonse, B., Jamtveit, B.: Microstructural records of
486 earthquakes in the lower crust and associated fluid-driven metamorphism in plagioclase-rich
487 granulites. Journal of Geophysical Research: Solid Earth, 123, 3729–3746.
488 <https://doi.org/10.1029/2017JB015348>, 2018
- 489 Petley-Ragan, A., Ben-Zion, Y., Austrheim, H., Ildefonse, B., Renard, F., Jamtveit, B.: Dynamic
490 earthquake rupture in the lower crust. Science Advances, 5, doi: 10.1126/sciadv.aaw0913, 2019.

- 491 Prior, D. J.: Sub-critical fracture and associated retrogression of garnet during mylonitic deformation,
492 Contributions to Mineralogy and Petrology, 113(4), 545–556, doi:10.1007/BF00698322, 1993.
- 493 Prior, D. J., Wheeler, J., Brenker, F. E., Harte, B. and Matthews, M.: Crystal plasticity of natural
494 garnet: New microstructural evidence, Geology, 28(11), 1003, doi:10.1130/0091-
495 7613(2000)28<1003:CPONGN>2.0.CO;2, 2000.
- 496 Prior, D. J., Wheeler, J., Peruzzo, L., Spiess, R. and Storey, C.: Some garnet microstructures: an
497 illustration of the potential of orientation maps and misorientation analysis in microstructural
498 studies, Journal of Structural Geology, 24(6–7), 999–1011, doi:10.1016/S0191-8141(01)00087-6,
499 2002.
- 500 Raimondo, T., Collins, A. S., Hand, M., Walker-Hallam, A., Smithies, R. H., Evins, P. M. and Howard, H.
501 M.: The anatomy of a deep intracontinental orogen, Tectonics, 29(4), n/a-n/a,
502 doi:10.1029/2009TC002504, 2010.
- 503 Shimada, M., Cho, A., Yukutake, H.: Fracture strength of dry silicate rocks at
504 high confining pressures and activity of acoustic emission. Tectonophysics 96, 159–
505 172. doi:10.1016/0040-1951(83)90248-2, 1983.
- 506
- 507 Sibson, R. H.: Generation of pseudotachylite by ancient seismic faulting, Geophysical Journal
508 International, 43(3), 775–794, 1975.
- 509 Sibson, R. H. and Toy, V. G.: The habitat of fault-generated pseudotachylite: Presence vs. absence of
510 friction-melt, in Geophysical Monograph Series, vol. 170, edited by R. Abercrombie, A. McGarr, H.
511 Kanamori, and G. Di Toro, pp. 153–166, American Geophysical Union, Washington, D. C. [online]
512 Available from: <http://www.agu.org/books/gm/v170/170GM16/170GM16.shtml> (Accessed 21
513 January 2014), 2006.
- 514 Toy, V. G., Ritchie, S. and Sibson, R. H.: Diverse habitats of pseudotachylites in the Alpine Fault Zone
515 and relationships to current seismicity, Geological Society, London, Special Publications, 359(1), 115–
516 133, doi:10.1144/SP359.7, 2011.
- 517 Trepmann, C. A. and Stöckhert, B.: Cataclastic deformation of garnet: a record of synseismic loading
518 and postseismic creep, Journal of Structural Geology, 24(11), 1845–1856, doi:10.1016/S0191-
519 8141(02)00004-4, 2002.
- 520 Voegelé, V., Cordier, P., Sautter, V., Sharp, T. G., Lardeaux, J. M. and Marques, F. O.: Plastic
521 deformation of silicate garnets, Physics of the Earth and Planetary Interiors, 108(4), 319–338,
522 doi:10.1016/S0031-9201(98)00111-3, 1998.
- 523 Vollbrecht, A., Pawlowski, J., Leiss, B., Heinrichs, T., Seidel, M. and Kronz, A.: Ductile deformation of
524 garnet in mylonitic gneisses from the Müncberg Massif (Germany), Tectonophysics, 427(1–4), 153–
525 170, doi:10.1016/j.tecto.2006.05.024, 2006.
- 526 Wang, Z. and Ji, S.: Deformation of silicate garnets; brittle-ductile transition and its geological
527 implications, The Canadian Mineralogist, 37(2), 525, 1999.
- 528 Wayte, G. J., Worden, R. H., Rubie, D. C. and Droop, G. T. R.: A TEM study of disequilibrium
529 plagioclase breakdown at high pressure: the role of infiltrating fluid, Contributions to Mineralogy
530 and Petrology, 101(4), 426–437, doi:10.1007/BF00372216, 1989.

531 Wex, S., Mancktelow, N. S., Hawemann, F., Camacho, A. and Pennacchioni, G.: Geometry of a large-
532 scale, low-angle, mid-crustal thrust (Woodroffe Thrust, central Australia): Geometry of a mid-crustal
533 thrust, *Tectonics*, doi:10.1002/2017TC004681, 2017.

534 Wex, S., Mancktelow, N. S., Hawemann, F., Camacho, A. and Pennacchioni, G.: Inverted distribution
535 of ductile deformation in the relatively “dry” middle crust across the Woodroffe Thrust, central
536 Australia, *Solid Earth*, 9(4), 859–878, doi:10.5194/se-9-859-2018, 2018.

537 Wex, S., Mancktelow, N. S., Camacho, A. and Pennacchioni, G.: Interplay between seismic fracture
538 and aseismic creep in the Woodroffe Thrust, central Australia – Inferences for the rheology of
539 relatively dry continental mid-crustal levels, *Tectonophysics*, 758, 55–72,
540 doi:10.1016/j.tecto.2018.10.024, 2019.

541

542

543

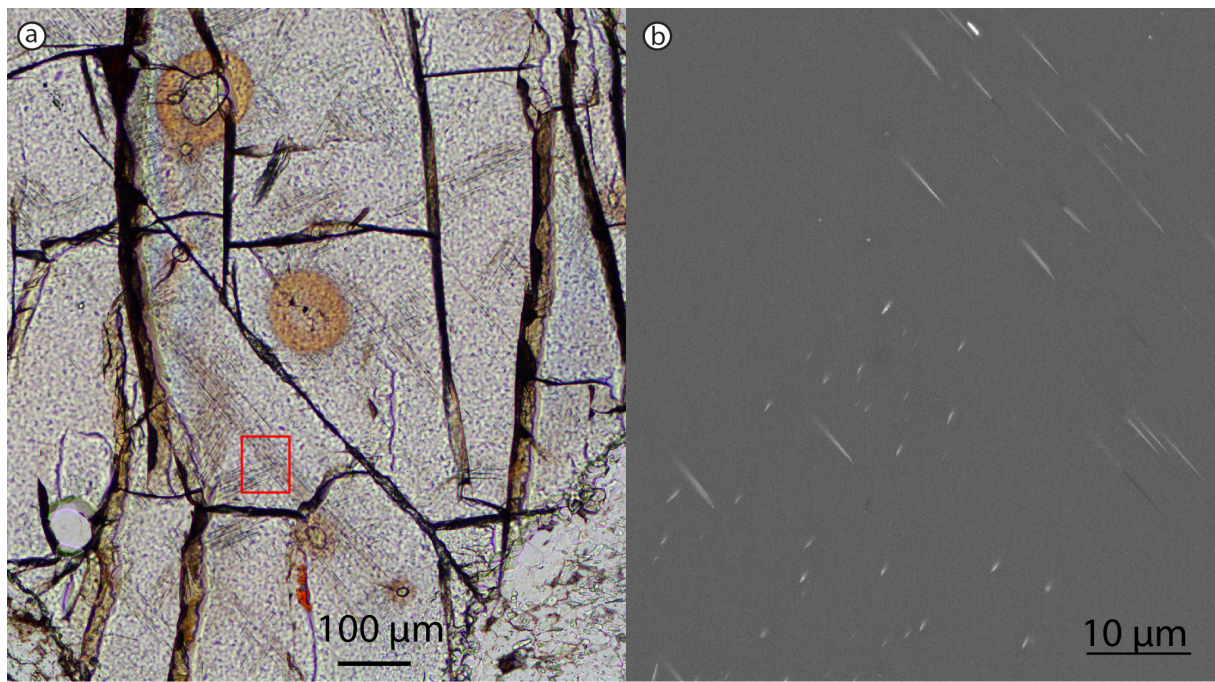
544

545

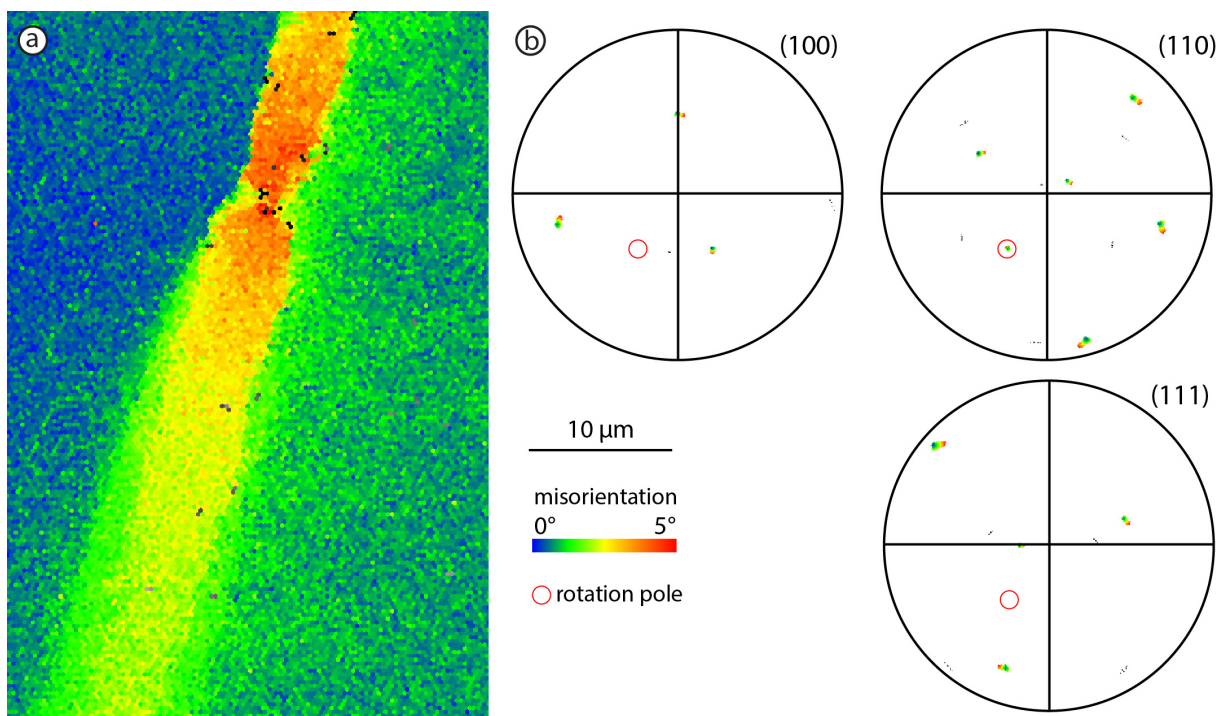
546

547

548 **Appendix**



550 *Figure A1: Thin section image in plane polarized light of a garnet crystal with monazite*
 551 *inclusions (with halos) and rutile-exsolution needles. b) BSE-image of the area indicated with*
 552 *the red box.*



554 *Figure A2: a) Misorientation map-detail for Fig. 6b), with b) pole figure plots for garnet axis*
555 *with the same colour scheme. The plots reveal a rotation around a (101)-axis, as indicated by*
556 *the red circle.*